

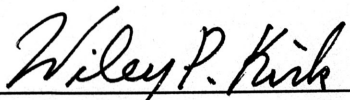
**INVESTIGATING RESONANCES IN BIPOLAR QUANTUM
RESONANT TUNNELING DEVICES**

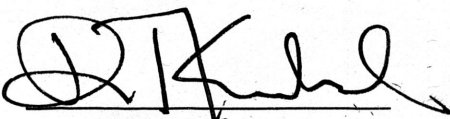
An Honors Thesis

by

Erik E. DeJongh

Approved as to style and content by:


Wiley P. Kirk, Advisor


Head of Honors Programs

April, 1993

ACKNOWLEDGEMENTS

Acknowledgement is due to my advisor, Professor Wiley P. Kirk, for his guidance, patience, and laboratory resources he provided for me. His advice and assistance are sincerely appreciated.

A debt of gratitude is owed to Dr. Alan Seabaugh, of Central Research Laboratories, Texas Instruments, for providing the samples, and helpful advice.

Thanks are also due to Dr. Craig Andrews, Kevin Clark, Feng Li, Robert Kilma, and Dr. Tifei Wang, for invaluable help in the laboratory.

Finally, acknowledgement is due to Larry Obee and the Helium Liquefaction Facility staff for providing the liquid helium, and to the Physics Department, Machine Shop and Electronics Shop staffs for invaluable assistance.

ABSTRACT

In this thesis, transport in Bipolar Quantum Resonant Tunneling Transistors (BiQuaRTTs) is studied. A ^4He cryostat was built, and ^3He - ^4He dilution refrigerator was modified for this work. Preliminary results in these experiments show multiple resonant peaks in the common-emitter current voltage characteristics, but fewer of these than a different sample structure reported in a previous unpublished study. Further studies are planned for Summer 1993 to resolve several interesting effects not previously reported.

TABLE OF CONTENTS

CHAPTER I	
INTRODUCTION	1
CHAPTER II	
TRANSPORT FUNDAMENTALS	4
CHAPTER III	
PREVIOUS STUDIES OF RTTs	13
CHAPTER IV	
EXPERIMENTAL APPARATUS	19
CHAPTER V	
EXPERIMENTAL PROCEDURES	29
CHAPTER VI	
RESULTS AND DISCUSSION	35
CHAPTER VII	
CONCLUSIONS	43
REFERENCES	44

CHAPTER I

INTRODUCTION

Current integrated circuit technologies are rapidly approaching their limits. Long term improvement in VLSI (Very Large Scale Integration) integrated circuits face several daunting problems. Interconnection limitations will limit minimum lateral device dimensions to approximately 0.25 micrometers, and with this, circuit packing density. Presently, scaling strategies are encountering difficulties with parasitic effects. The cost of improving this technology is also a limitation: upgrading one industrial integrated circuit fabrication facility to build integrated circuit components with minimum line widths of 0.5 micrometers to 0.25 micrometers will cost several billions of dollars (for instance, x-ray lithography). If the industry is to continue to grow, it must explore other novel technologies.

In the last decade, vast improvements in fabrication and materials development have been made. Epitaxial techniques allow fabrication of vertical features an atomic layer in thickness, and advanced lithography can define lateral dimensions on the order of several tens of nanometers.

These make feasible the fabrication of electron devices that operate purposefully in the domain of quantum mechanics. In recent years, the industry has greatly stimulated research efforts focused upon quantum-effect devices.

Today, there are a wide variety of devices under study at corporate and university laboratories worldwide. These include superlattice devices, quantum well lasers, resonant tunneling diodes (RTD's), numerous types of quantum-effect transistors, and quantum dot RTD arrays to name a few. Resonant tunneling transistors in particular, (RTTs) appear to hold much promise in device applications.

In 1984, Cappasso and Kiehl [1] originated the idea of a resonant tunneling bipolar transistor (RTBT). This device would exhibit resonant behavior in its current-voltage characteristics, like the resonant tunnel diode, but it offers gain, and input-output isolation. They saw immediate applications for their device, like A-D converters, oscillators, parity generators/checkers, and frequency multipliers. Capasso's group at Bell Labs produced the first operating RTBT, and have since tested many different device configurations.

In 1988, Seabaugh and his coworkers at Texas Instruments designed a resonant tunneling bipolar heterostructure transistor with superior common-emitter characteristics to those of Capasso's group. The BiQuaRTT is a very robust device showing strong room temperature current peaks, peak to valley ratios, and DC gains. Multiple negative differential resistance (NDR) in the common-emitter current-voltage characteristics result from the strong modulation of the transmission coefficient with the base-collector voltage, as will be described in chapter 2.

Recently, wide-base BiQuaRTTs were reported to exhibit a greater number of NDR peaks than simple quantum mechanics predicts. To further investigate this phenomena, wide-base BiQuaRTT samples were provided by Texas Instruments Central Research Laboratories to the NanoFAB Center for this research.

The objective of this work is to investigate this effect, and BiQuaRTT transport characteristics in general. An enhanced understanding of transport in the BiQuaRTT may lead to device performance improvements and may reveal ways to further utilize its transport phenomena.

CHAPTER II

TRANSPORT FUNDAMENTALS

In this chapter, transport phenomena and properties germane to the BiQuaRTT are briefly discussed. A number of texts treat heterostructure bipolar transistors (HBT)s exclusively, and more detailed discussions on recombination and scattering abound.

Band diagrams for a HBT are shown in figure 1. HBT's utilize a wider bandgap material in the emitter than in the base. This is favorable for injected electrons from the emitter, and resists hole currents from base to emitter, thus improving emitter injection efficiency. This also allows a lightly doped emitter, high doping and a very thin base without increasing base sheet resistance, resulting in decreased base scattering.

In a npn HBT (includes BiQuaRTTs), there are several recombination mechanisms important to such a structure.

Intrinsic recombination processes are band to band processes that do not depend upon an intermediate state, like a defect or an impurity, to occur. These are generally termed radiative recombination because they involve conduction electron-valence hole annihilation, resulting in the

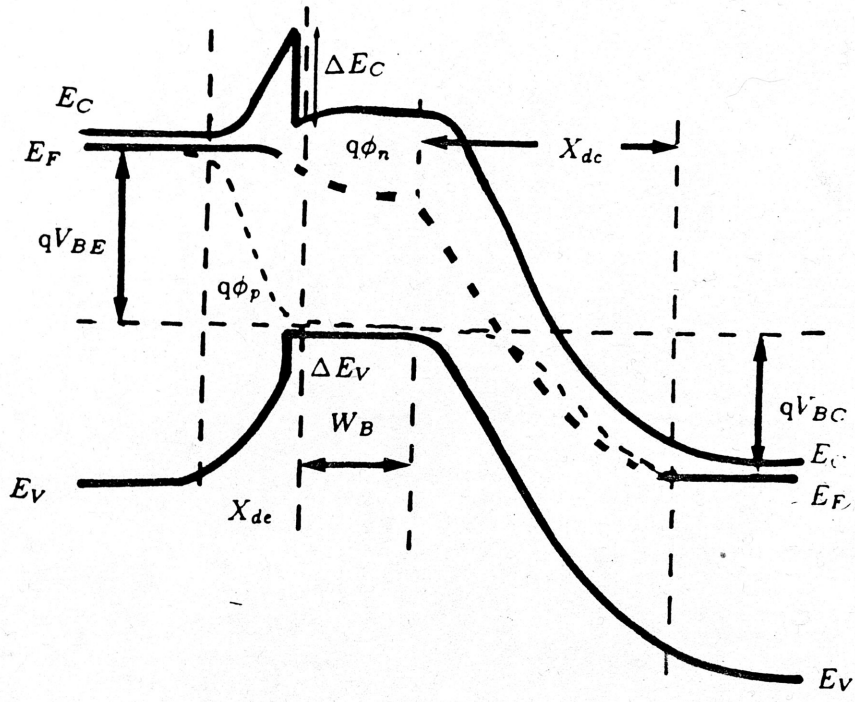
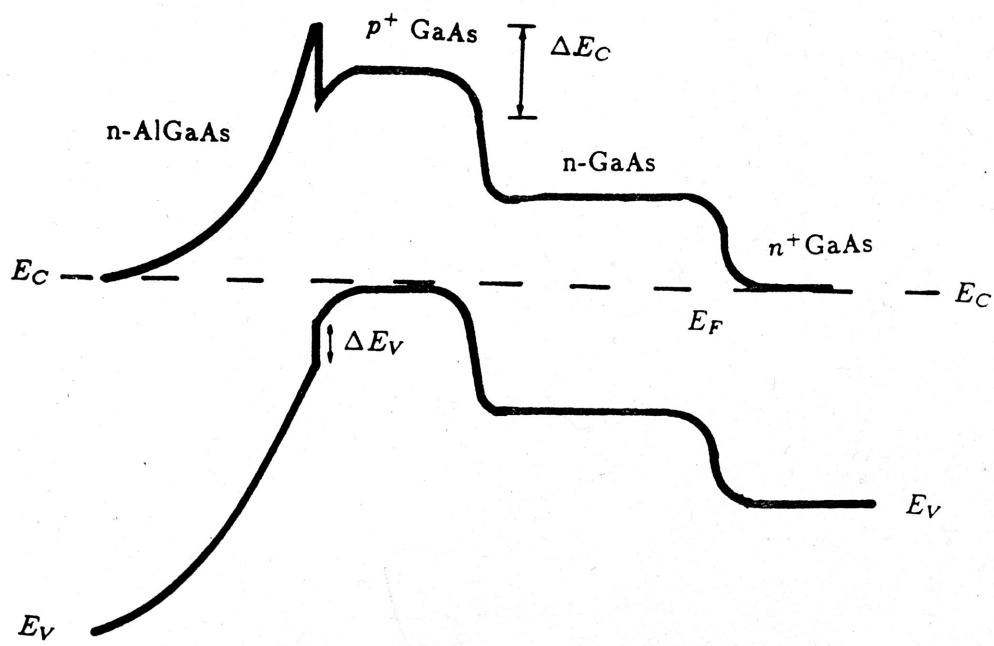


Figure 1. Band diagram at a HBT [2].

emission of a photon. Since one identifies a hole as the lack of an electron in a lattice covalent pair bond (valence band), which is mobile there and behaves as if itself a particle of opposite charge, it is easy to visualize an electron dropping down into this hole (bond) which fixes it in energy space in the valence band, upon which time the difference between its conduction band and the valence band energy (E_g) is radiated as a photon. For indirect gap semiconductors a phonon is required to supply the momentum for the lateral component of the band to band event. Such three particle events are many orders of magnitude less probable than direct radiative recombination.

As implied above, then, extrinsic recombination is that requires a mediating state to occur. Effective recombination centers (traps) reside close to mid-band gap and dramatically reduce minority carrier lifetimes. This type of recombination, also called Shockley-Read-Hall (SRH) recombination, can be shown for a npn HBT to possess a recombination rate of [2]

$$U_{SRH} \sim \frac{1}{2} \sigma v_{th} N_t n_i e^{\frac{q V_{BE}}{2kT}} \quad (1)$$

where the electron capture density is $\sigma_n = \sigma_p = \sigma$, the electron thermal velocity is $v_{th}^n = v_{th}^p = v_{th}$, n_t is the trap density, N_i is the intrinsic carrier density, and V_{BE} is the base emitter bias.

SRH recombination in HBT's is primarily due to fixed ionized impurities in the base-emitter depletion region. Here, the injected (diffusing) emitter electron density meet impurities which are ionized when the base-emitter depletion region extends over them.

A couple of comments are appropriate here: First, no equation (1) is provided for the collector junction, because the motive force there is drift - minority electrons after traversing the base are literally swept across the base-collector heterojunction. The collector, being a reverse-biased diode, only contributes a leakage current towards the base and emitter terminals. To see how important SRH recombination is in HBT operating characteristics, consider its emitter efficiency

$$\gamma = \frac{I_E^n}{I_E^n + I_E^p + I_{rg}} \quad (2)$$

where I_E^n is the injected emitter electron current, I_E^p is the hole current from base to emitter, and I_{rg} is the current due to recombination and

generation (opposite of recombination). I_{rg} is easily computed from equation (1) and has this same factor of two in the exponent. Since DC gain is proportional to the emitter efficiency, significant I_{rg} degrades device performance, and results in collector currents with this two in the exponent (ideality factor) for low currents.

At the other end of the collector current range is Auger recombination. This is a radiative mechanism in which a second electron is excited in the valence band by the emitted photon. This mechanism becomes important during high level injection - that is when injected excess minority carrier densities are non-negligible compared to majority carriers, or where high base doping is employed.

These mechanisms combine to define the bulk base recombination time (minority carrier lifetime), given by

$$\frac{1}{\tau_n} = \frac{1}{\tau_{SRH}} + \frac{1}{\tau_{AUG}} + \frac{1}{\tau_{RAD}} \quad (3)$$

where the terms on the right hand side are the bulk recombination times for each mechanism. From this, base diffusion length $L_n = \sqrt{D_n \tau_n}$

may be determined, to set a maximum base thickness for which, the current gain is not seriously degraded.

Another source of recombination in HBT's is surface recombination. Typically this is reduced using appropriate processing technology. It may be further lessened by using an emitter stripe to attain large emitter periphery to area ratio [2].

Electrons may suffer collisions as they traverse the device. The relaxation time approximation describes scattering collisions as occurring at time intervals of a mean free time and distances of a mean free path, and carriers otherwise travel on the average at the drift velocity when influenced by an electric field related by

$$l_m = \frac{V_d}{\tau_m}$$

$$V_d = -\left(\frac{q\tau_m}{m^*}\right)E = -\mu_n E \quad (2)$$

where μ_n is the electron mobility, m_* is the electron effective mass, E is an electric field providing acceleration between collisions. The most

important way this scattering manifests itself is in limiting carrier mobility.

Important scattering mechanisms are ionized impurity scattering, lattice scattering, and in some applications, carrier-carrier scattering.

Ionized impurity scattering arises from Columbic interactions between mobile carriers and fixed ionized impurity atoms (ionized in the space charge region at a semiconductor homo- or heterojunction). This is referred to as the depletion approximation; it holds that all atoms in this depleted zone are ionized. This scattering mechanism can be shown to limit mobility to proportionality to $T^{3/2}$ [3]. At higher temperatures, carriers on average move faster, and are thus less deflected by ionized impurities. This mechanism tends to dominate mobility at low temperatures.

Lattice or phonon scattering is another important mobility limiting interaction. Phonons are quantized lattice vibrations which cause local variations in conduction and valence band edge energies, thus exchanging a quantity of kinetic energy for potential energy. A quantum mechanical calculation [3] obtains mobility proportional to $T^{-3/2}$, but are empirically observed to deviate from this, even in the temperature region in which

this behavior is the dominant mechanism. This is because there are two modes of phonons acoustic (low frequency) and optic (high frequency).

The $T^{-3/2}$ dependence is when only acoustic phonons are considered.

The optic mode yields a mobility dependence of $\frac{1}{T} e^{-\frac{h\omega_{OP}}{2\pi kT}}$ where

$\frac{h}{2\pi}\omega_{OP}$ is the phonon momentum, with this dependence applicable

when $T < \frac{h\omega}{2\pi k}$. For compound semiconductors, atoms carry ionic

charge, thus their displacement is an electric polarization. These polar, longitudinal optic modes produce a temperature dependence, of $\frac{1}{T} e^{-\frac{h\omega_{OP}}{2\pi kT}}$ with an empirical coupling constant as a pre-multiplier.

For semiconductors with multiple conduction band minima, two possibilities for scattering arise: intravalley scattering between two conduction band valleys yielding $T^{-3/2}$ dependence, and intravalley scattering within a conduction band minimum, but often involving a significant change in electron wave vector (momentum), yielding a

$\frac{1}{T} e^{-\frac{h\omega_l}{2\pi kT}}$ dependence.

The Columbic interaction between carriers is only important at very high current densities, in which case high level injection effects as mentioned earlier, tend to dominate.

Finally, a brief mention of tunneling is in order. Tunneling is a quantum-mechanical effect involving the wavelike properties of electrons (and holes). An electron is described by a wave function whose modulus is a probability density. If a given electron is caused to impinge upon a sufficiently thin potential barrier, the probability density will extend to the opposite side of the barrier. If there is an available state on the opposite side, the electron may tunnel through. Due to the probabilistic nature of quantum mechanics, one may not know with certainty whether the given electron will tunnel, or be reflected, but a transmission probability can be calculated which would characterize the collective behavior of large numbers of electrons (i.e., calculate the transmitted current).

CHAPTER III

PREVIOUS STUDIES OF RTTs

In 1986, F. Capasso's group at Bell Labs produced the first operating bipolar resonant tunneling transistor, employing thermionic emitter injections [5], after earlier proposals utilizing ballistic and hot electron injection proved too difficult to design to yield room temperature resonant tunneling (RT). These earlier designs were at first emphasized because they do not involve bias across the well barriers, which would destroy symmetry between the two barrier heights, and thus reduce peak to valley ratios through loss of phase coherence in the well [6]. Capasso's GaAs/AlGaAs devices have exhibited typical room temperature peak to valley (P/V) ratios of approximately 2.0 with DC current gains of 7-10 [6].

In 1988, A. C. Seabaugh's group at Texas Instruments developed another structure, which they named the Bipolar Quantum Resonant Tunneling Transistor (BiQuaRTT). A calculated BiQuaRTT band diagram is shown in figure 2. This structure accomplishes RT by modulation of the base-collector tunnel barrier transmission coefficient with the

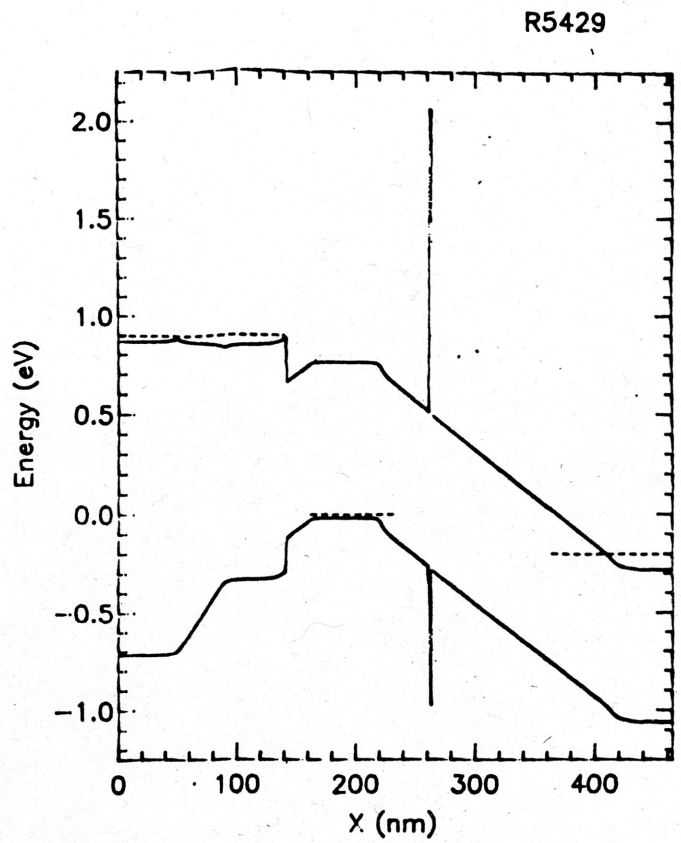
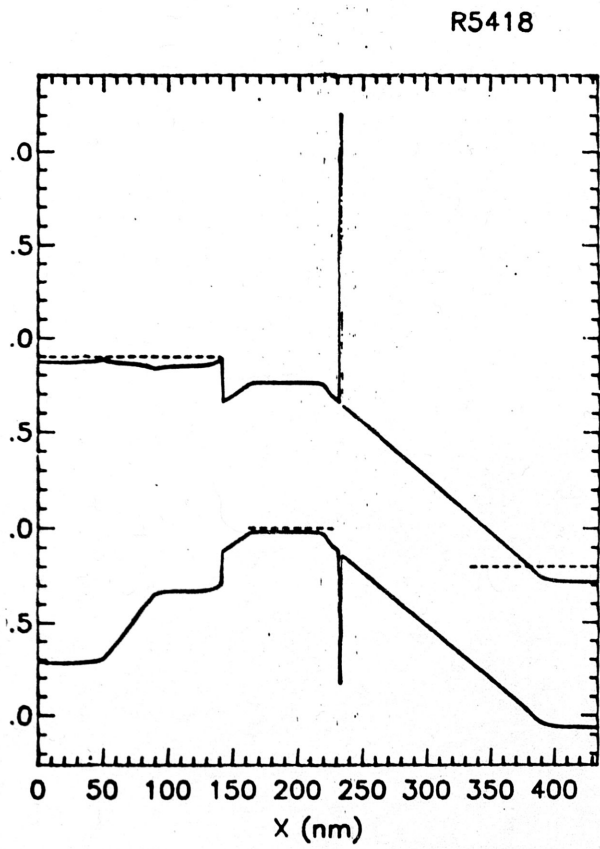


Figure 2. Band diagrams of two BiQuaRTT devices.

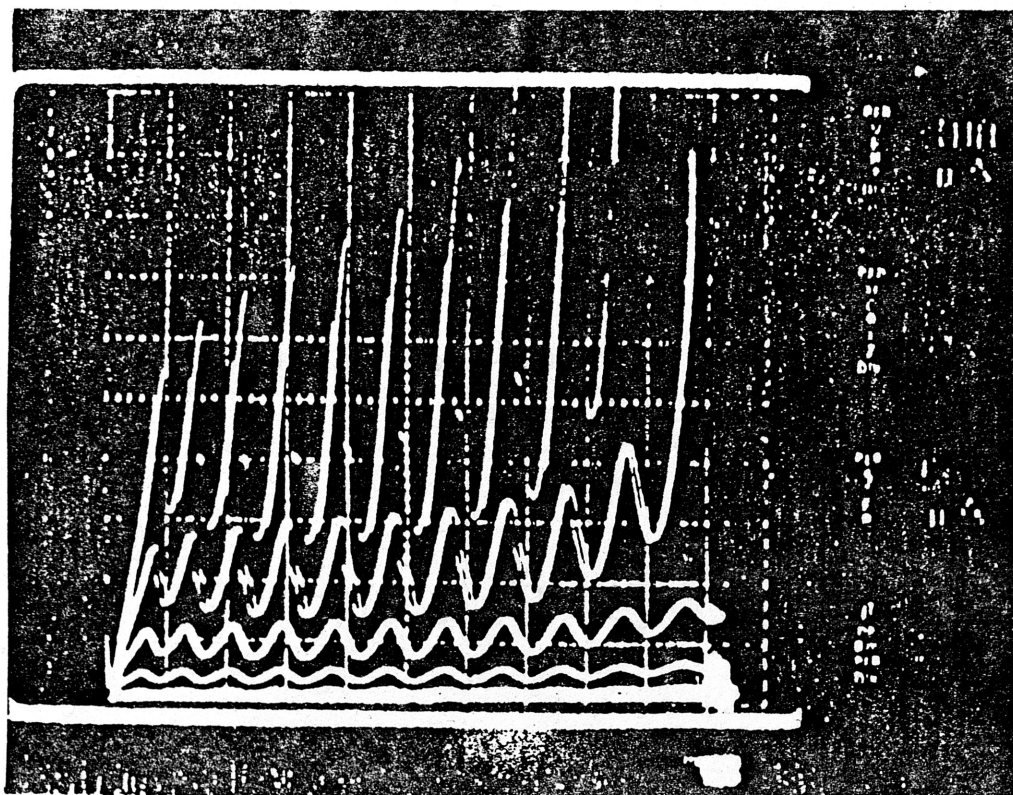
collector-base bias. The group measured P/V of more than 2.0 with DC current gains of 10 to 50, while exhibiting multiple negative differential resistance (NDR) [7]. This NDR arises as follows: electrons are injected into base quasi-bound states, and diffuse across the base. The distribution being broader than the separation between base states, quasi-thermalizes (fall to lower base states by emission of a phonon), to form a narrow distribution near the triangular notch on the collector side of the base. As collector-base bias is increased from a current peak, the lowest base states with electron wavevector parallel to the current density drops into the triangular notch, thus distributing the thermalized distribution amongst higher momentum states of lower transmission probability (greater effective barrier width). Hence the modulation of the transmission coefficient in the triangular notch give rise to the NDR regions [7]. This approach gives rise to less asymmetry between the two barrier heights at a given bias, and reduces the flat-band voltage, than if base emitter voltage was used to modulate transmission by alignment of emitter electron distribution to base well states as in Capasso's devices.

Bipolar RTT's have interesting and very promising electronics applications. Prominent among these is multiple-valued logic applica-

tions. A number of investigators have demonstrated this capability in RTD's [8]-[11], but these lack input-output isolation and I-V reproducibility of a transistor. Recently, Capasso's group demonstrated this capability with a bipolar RTT producing two peaks and hence three logical levels. Capasso's group has also demonstrated frequency multipliers, scrambling circuits, a 4-bit parity generator, and an analog to digital converter [4]. Even more impressive, is Seabaugh's demonstration of logic function compression by building an XNOR circuit from one resonant hot electron transistor and bias resistor, replacing a nine transistor circuit .

Recently, Seabaugh and colleagues, observed more I-V peaks in a wide-base BiQuaRTT device than the quantum mechanics of the triangular potential well predicts, as shown in figure 3. The well may be approximated as an infinite triangular well whose eigenfunction is well known,

$$E_n = \left(\frac{\hbar^2}{2m^*} \right)^{\frac{1}{3}} \left(\frac{3\pi a}{2} \right)^{\frac{2}{3}} \left(n + \frac{3}{4} \right)^{\frac{2}{3}} \quad (1)$$



R5429

40 nm

Figure 3. Observance of unexpectedly numerous peaks in a BiQuaRTT.

where m^* is the electron effective mass, a is the slope of the well, and n is an integer ($n=0, 1, 2, \dots$). The well slope a is the vehicle for transmission probability modulation in its dependence upon base-collector bias (V_{BC}), and is determined from self-consistent band calculations. Seabaugh's group found excellent agreement between this calculation and experimental data for narrow-base devices.

This discrepancy in device characteristics could be due to virtual coupling between the triangular well, and a smaller triangular notch on the emitter side of the base.

Investigation of this interesting phenomena, as well as transport in general in wide-base BiQuaRTTs are of central importance in this research.

CHAPTER IV

EXPERIMENTAL APPARATUS

In order to investigate the magnetotransport properties of the BiQuaRTT, temperature and magnetic field must be varied. Transport properties in any device determined from observation are typically recognized or identified from temperature, field, current, etc ..., dependencies and correlations contained in empirical data. These often impose stringent conditions which must be met by the measurement apparatus through careful design of both equipment and experiment. This chapter describes the former in reference to this research.

A. ^4He Cryostat

The primary means for making transport measurements for this work is a ^4He dip cryostat, consisting of a dewar housing, a magnet, and an insertable sample probe. Liquid ^4He fills the dewar, comprising a 4.2 K thermal reservoir which cools the sample, and an AMI model 4105 superconducting solenoid magnet. ^4He bath level may be monitored from an AMI model 125 superconducting level sensor and model 101 level

meter. Four radiation baffles provide partial isolation between the helium bath and the top flange at room temperature. Brass shims are employed to pass the magnet current around the baffles to 50/50 tin-lead solder coated Cu 20 AWG braids which connect to the magnet.

The magnet is rated at 79 kG @ 78A, but is used to 6T (60 kG) here. The dewar and magnet is protected from damage in case of quenching by a ring of high current diodes located on the magnet body. These diodes are also employed through a persistent switch, to change the magnitude of the flux density. In this study, data will be taken with the magnet in its persistent mode i.e. at constant B, for values of 1, 2, 4, and 6T at sample temperature to 20 K.

The sample probe from the dip cryostat, built by the author, is shown in figure 4. It consists of a 43" long, 1/2" diameter stainless steel tube silver soldered to brass flanges at both ends. A quick-connect fitting on this tube slides up and down, allowing raising and lowering slowly, without losing helium gas from the bath. At the lower end, the sample, sample holder, and thermometry are all contained within a non-magnetic hermetic can which is lowered into the magnet bore for measurement taking. Helium is used as a heat exchange gas to transfer heat from the

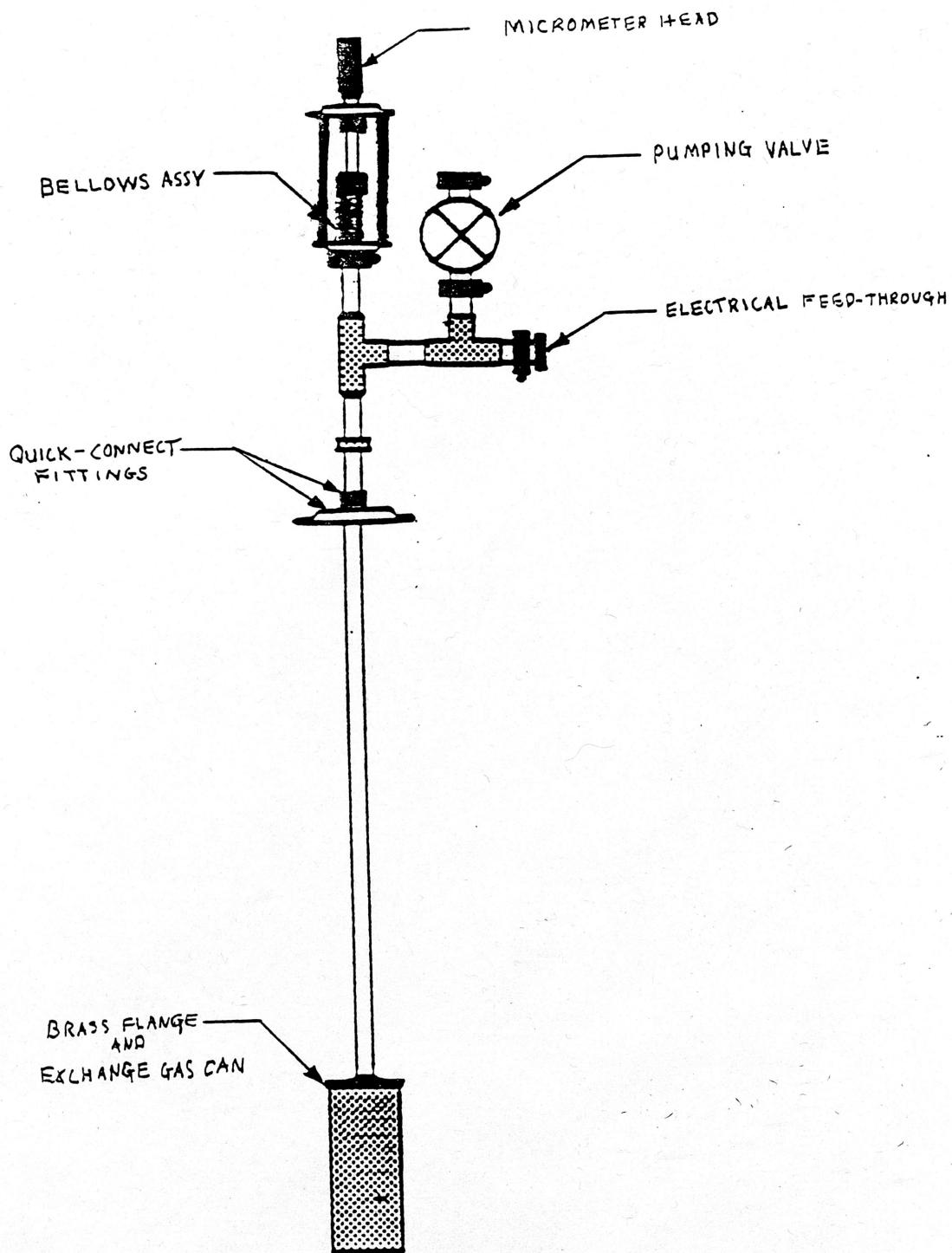


Figure 4. Schematic diagram of a dip probe.

sample and holder to the bath, and is pumped out through the stainless tube and a valve at the top of the probe, when measurements at intermediate temperatures are taken in conjunction with the running of the magnet.

Figure 5 shows details of the experimental space inside the exchange gas can. The sample holder assembly consists of a coin silver sample platform, pivoting on Be-Cu pivot screws and held in a coin silver frame. The platform is actuated at the top of the probe, by a 1" micrometer head through a roller bearing and Cu bellows assembly to a Cu-Ni 1/8" diameter tube, and finally a 0.010" nylon line. Tension is maintained by a non-magnetic stainless steel spring. The sample holder frame bolts directly to an OFHC Cu heater spool with Cu powder-impregnated Apiezon-N grease to improve thermal contact by filling surface irregularities. The heater, 110 Ω from 0.005" Neutroloy resistive wire, is employed to heat the sample from 4.2 K, when the magnet is used, thus prohibiting raising the probe out of the bath.

When no exchange gas is used, the sample apparatus is thermally isolated from the 4.2K flange above it by four nylon support rods, and the nylon actuating line, save for the sample leads. Heat sinking of metal wires is important in any cryogenic application, because they can contrib

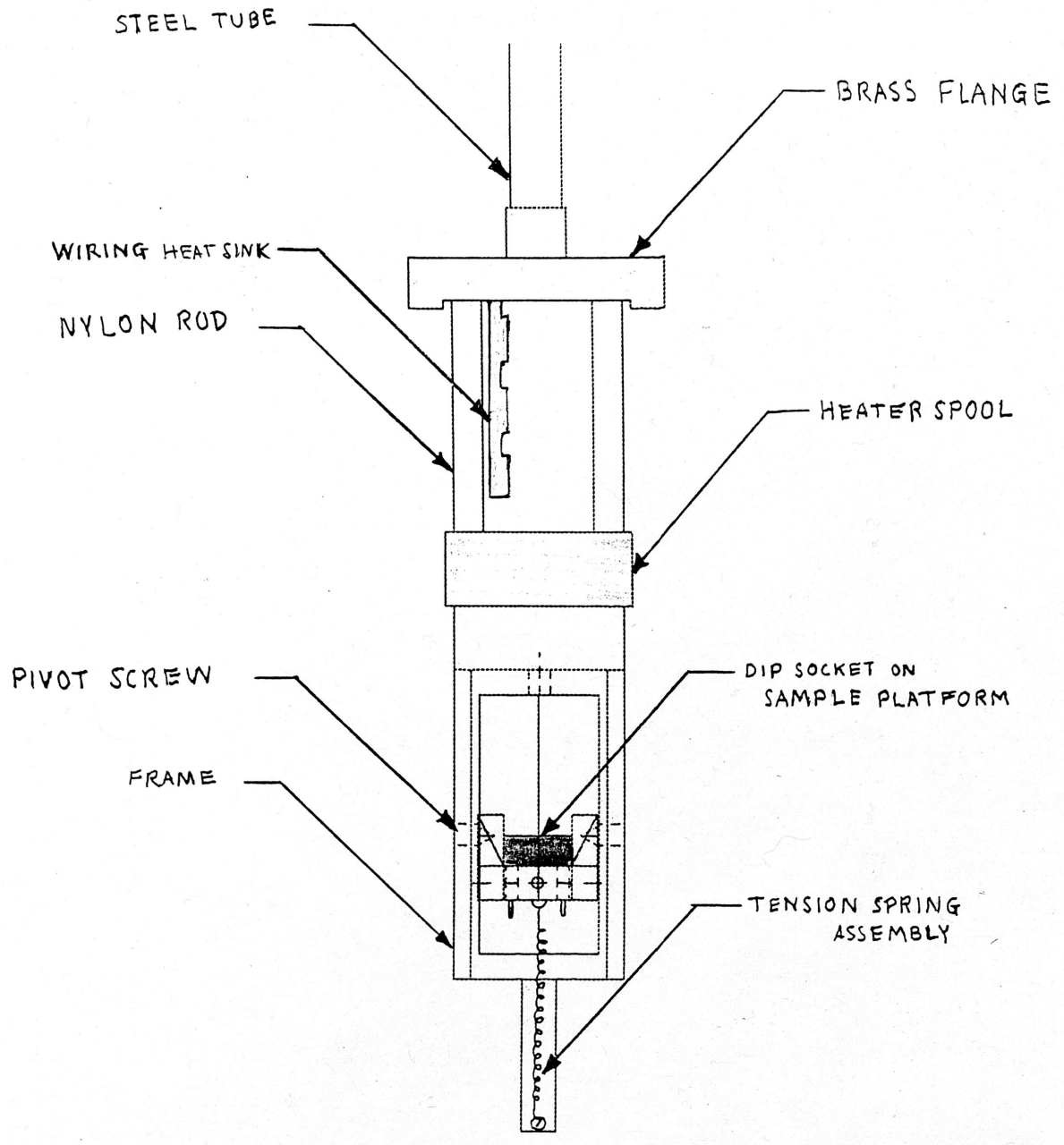


Figure 5. Detail of dip probe experimental stage.

ute sizeable heat links. For this application, the sample leads provide the thermal link to the 4.2 K flange, and are heat-sunked to this flange with Stycast 2850GT epoxy (K approximately that of brass).

The probe and cryostat apparatus enables measurements from 1.8 K (by pumping on the bath) to room temperature, or 1.8 K to 20 K when using the magnet (immersed necessarily in the ^4He bath). Temperature is monitored by a MTI Research CC-1000 Carbon-glass resistance thermometer, thermally anchored to the sample holder frame with an OFHC Cu cylinder and Stycast 2850 GT epoxy.

B. Dilution Refrigerator

The dilution refrigerator modified by the author is represented schematically in figure 6. It is a previously in house-built cryostat using a modified SHE 220 dilution refrigerator insert. The device reaches millikelvin temperatures by the entropy change of mixing from diluting ^3He into ^4He .

A ^3He and ^4He gas mixture is admitted to a heat exchanger in the 1 k pot ($T=1.1\text{k}$ by pumping on liquid ^4He). The incoming $^3\text{He} - ^4\text{He}$ mixture, called the mash, forms the dilute side of the circulation. The

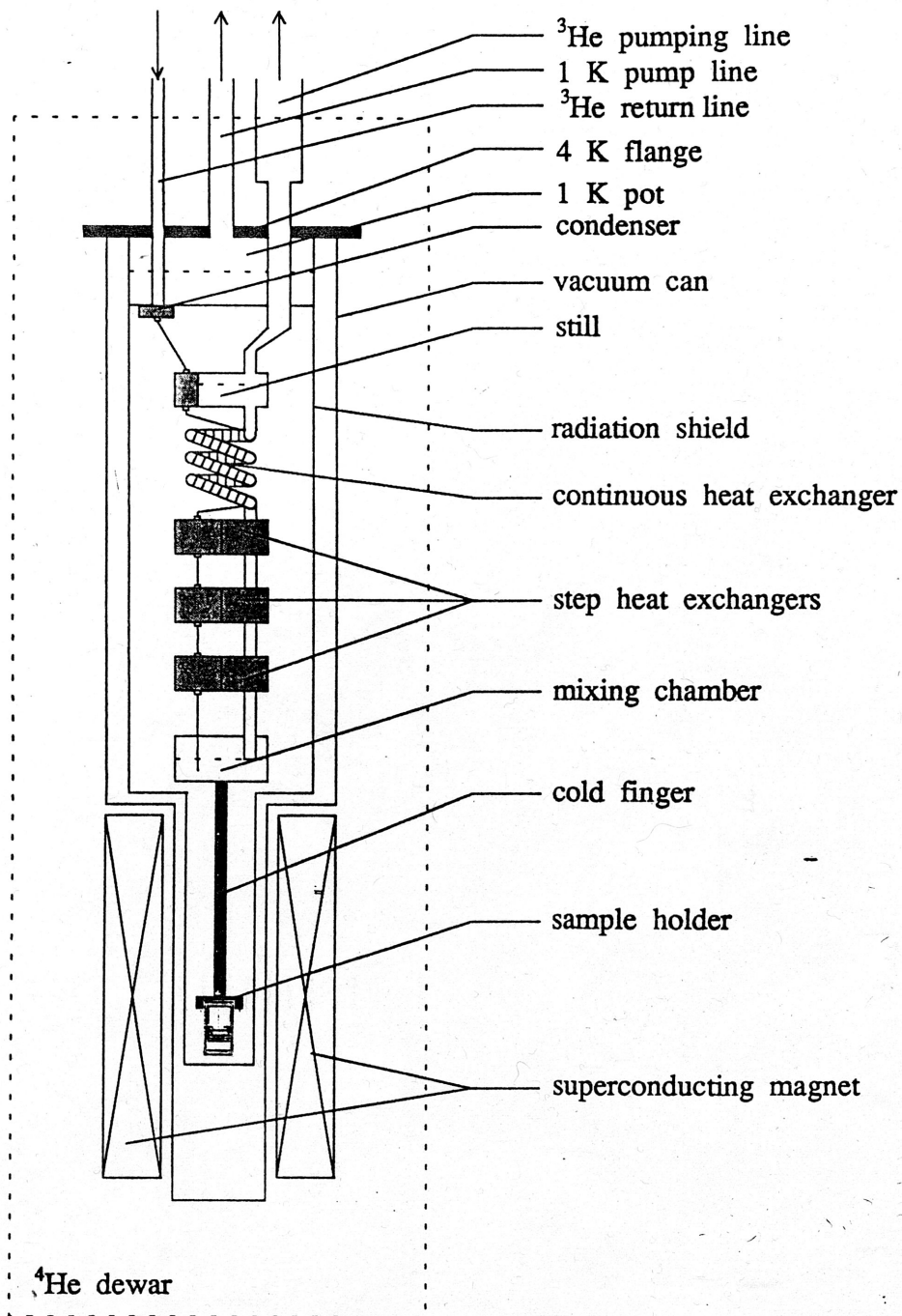


Figure 6. Schematic diagram of a dilution refrigerator [13].

precooled mash liquifies via a flow impedance, and then enters the still heat exchanger at approximately 0.7 K, followed by the continuous heat exchanger, and the discrete heat exchangers. The liquified mash then enters the mixing chamber and crosses the dilute - concentrated phase boundary. The concentrated ^3He phase, being lighter, floats on the dilute phase. Upon mixing, an entropy increase results in an absorption of heat. ^3He atoms are then osmotically driven through the heat exchanger (concentrated side), to the still. ^4He being a boson, is a superfluid under these conditions, and thus fills up the heat exchangers to the still; the ^3He diffuses through this to the pumping orifice. Heating the still, use of an impedance or in some cases a still pumping orifice film burner combine to maintain a high partial pressure of ^3He and a low one for ^4He , thus increasing circulation. The ^3He (>90% ^3He) is then pumped away at the still, further cooling the still.

A dilution refrigerator may be operated as a ^3He cryostat to sample temperatures in excess of 150 K.

The refrigerator has been fitted with a micrometer-controlled swinging sample platform as in the dip probe, and modifications were made to accommodate the same magnet.

C. Instrumentation

The measurement electronics for the dip cryostat include two Kiethley 220 current sources, an ICS4831 4-channel voltage source, a Kiethley 617 electrometer used as an ammeter, and three Hewlett-Packard 3478A digital multimeters. All of these are interfaced to a PC through an IEEE-488 interface bus, allowing them to be controlled with simple computer programs. The magnet is powered by a Kepco 100M regulated DC power supply, a power amplifier, and controller built by a former student.

The electronics for the dilution refrigerator, are much the same as for the dip cryostat except for temperature measurement. A carbon glass resistor (Lakeshore CGR-1500) is used for higher temperature ranges (allowing simple 4 terminal DC measurement), but below 1.2 K, its resistance becomes virtually infinite. Under these circumstances, carbon resistors are used with lock-in amplifier and AC resistance bridge. This is necessitated by the stringent constraints a refrigerator imposes upon heat leaks. A Brookdeal Ortholoc lock-in amplifier is employed as a null detector with an AC resistance bridge built by a previous student and a Singer Ratio Standard seven decade ratio transformer to measure the

resistance of five Speer carbon resistors at the 1 K pot, still, the continuous, first and fifth step exchangers, and the mixing chamber, as well as a Matsuhita carbon resistor in the mixer.

The aforementioned thermometry are calibrated to two superconducting fixed point thermometers (NBS # SRM767 & SRM768). During precooling, bath temperature is monitored with a Lakeshore DT370 silicon diode.

For the refrigerator, the magnet is powered by two Hewlett-Packard 6295B DC power supplies arranged as master-slave, and a Kepco Bipolar 12M DC power supply to allow negative polarity offset currents, and controlled by an IEEE-488-interfaceable controller, built by a former student. The persistent switch arrangement is identical to that of the dip-cryostat.

CHAPTER V

EXPERIMENTAL PROCEDURES

In this chapter, the operating procedures utilized in these studies are described. These include a dip-type ^4He cryostat and $^3\text{He}/^4\text{He}$ dilution refrigerator both located at the NanoFAB Center at Texas A&M.

A. Dip Cryostat

The dip-probe cryostat described in chapter 4 was heavily relied upon for the experimental measurements presented in chapter 6. Its operation is greatly simplified compared to the dilution refrigerator, and it allows a far wider temperature range, save for the operation of a magnet.

The cool down process for this cryostat entails first flushing the dewar with nitrogen gas, followed by transferring liquid nitrogen. A silicon diode (Lakeshore DT-370) mounted on the magnet, being the most thermally massive object in the cryostat, is monitored periodically until it indicates a temperature of 80-85 K. The liquid N_2 is then back-transferred and the dewar is pumped out to eliminate residual nitrogen which

would boil away liquid helium. Next, the dewar is flushed with ^4He gas followed by the transfer of liquid ^4He to comprise the bath. When the magnet is fully immersed, a sample probe may be inserted and then measurements can begin.

Prior to inserting the probe, a continuity check is completed, and its exchange gas can be installed, evacuated, and leak-tested. This procedure may be repeated numerous times during one cool down cycle, allowing characterization of many samples in a short time span.

Normally, probe temperatures are varied by raising the probe from the bath into the cold helium gas above it, through a suitable exchange gas (e.g., helium) to transfer heat to/from the sample. When measurements involving the magnet are desired, the magnet controller is manually operated to energize the magnet through a number of high current-rated diodes comprising part of the persistent switch. If a constant magnetic field is desired, its magnitude is set, and the persistent switch is turned off, yielding a persistent current in the magnet.

Performing measurements using the magnet, and raising sample temperatures above that of the bath requires a heater, since the probe must reside in the magnet bore and the magnet must remain immersed in

the bath. The use of a heater in such proximity to the bath results in large thermal gradients which limit 3 sample temperatures in this apparatus to about 20 K for such measurements.

Two BiQuaRTT measurement runs were carried out with this cryostat in the manner just discussed for zero magnetic field. Results of these are presented in chapter 7.

B. Dilution Refrigerator

The $^3\text{He}/^4\text{He}$ dilution refrigerator described in the last chapter was run before its modification was complete to evaluate its performance and identify any problems. This section describes in a fairly general manner, the operating procedure for most dilution refrigerators.

The first order of business in a measurement run on a dilution refrigerator is to perform continuity tests and mount the sample. A typical refrigerator has more than 200 very fine leads, which are easily damaged when the dewar, magnet, exchange gas can, and thermal shields are removed or installed.

Next, the entire refrigerator should be leak-tested, usually with a mass-spectrometer leak detector as in the NanoFAB Center. If no leaks

are found, the dewar is then raised into place, and pumped on. The exchange gas can also be pumped out; both tasks require at the very least, several hours. Once the pressure in the dewar reads about 20-50 $\mu\text{m Hg}$, the 1 K pot is pumped on. Then, both sides of the circulation system is pumped on, followed by installation of a liquid nitrogen cold trap, to trap any contaminants when circulation is initiated. Now, circulation is started to determine if there are any restrictions in the plumbing. Here, the circulation pump is closed off, and the rise time between two pressure measurements determines the circulation rate. Next, the dewar and the exchange gas can are filled with nitrogen gas, with the 1 K pot fill valve open.

After closing the 1 K post pumping valve, liquid nitrogen is transferred into the dewar. The diode thermometer on the exchange gas can is monitored until it indicates that the refrigerator insert is at 80-90 K. The liquid N_2 is then back-transferred out, and the 1 K pot, dewar, and exchange gas can are all pumped out.

Once the back-transfer process is completed, helium gas is admitted into the dewar, and the exchange gas can is leak-tested again. Then, the 1 K pot fill valve is closed and it is pumped out to remove any residual

nitrogen gas. The fill valve is then opened to admit ^4He gas, with the pump valve closed. Now liquid helium may be transferred.

While the transfer tube is cooling, H_2 gas is admitted into the exchange gas can, to transfer heat from its contents to helium bath. The transfer rate is carefully controlled to avoid freezing the H_2 gas (pressure drops dramatically) above 23 K, because this would make it difficult for the 1 K pot to cool the refrigerator enough to achieve phase separation of the mash. When the level sensors indicate the ^4He both is full, the 1 K pump valve is opened and then closed, monitoring its pressure to check for restrictions.

Finally, more than 24 hours after mounting the sample, circulation is initiated. The 1 K pot is pumped on with the fill line still open, to obtain a temperature of approximately 0.9 K, and is the coldest part of the apparatus. The mash is then condensed in several steps, due to the limited capacity of the 1 K pot. The thermometry are monitored until the base temperature is achieved, and measurements can then begin, interrupted by daily helium transfers to maintain the bath.

In performing the tests described above, two problems were discovered. First, the transfer tube, being isolated from room tempera-

ture with a vacuum jacket, was found to be somewhat soft (would not hold a hard vacuum), thus slowing the transfer process and consuming an inordinate quantity of liquid helium. Second, some nitrogen remained in the 1 K pot during transfer, resulting in a very small constriction. This caused the 1 K pot to go dry after only two days of continuous running. After this circulation ceased and the 1 K pot and mixing chamber temperature rose, while the still temperature dropped while the mash was evaporating there, then it too began to warm to 4.2 K.

Measurements of BiQuaRTT magnetotransport with the dilution refrigerator are planned for summer 1993, subject to funding approval.

CHAPTER VI

RESULTS AND DISCUSSION

Current-voltage measurements carried out with the BiQuaRTT samples are described here.

First, preliminary measurements were done to try to observe the reported anomalously numerous peaks. In these samples, no such effect was observed. Four peaks were found for collector-emitter voltages from 0V to 5V throughout the temperature range 4.2K to 300K. Figures 7-10 show common-emitter characteristics of three of these devices. Figure 7a shows strong room temperature RT in device C4, typical of all of the sample devices. Below this, a single current-voltage (I-V) curve at 77K. This interesting trace exhibits significant current shift, and a slight voltage shift, between ramping the collector-emitter bias up, and then back down. This effect is only weakly influenced by base current beyond flatband, and is a strong function of V_{CE} . The shifts are almost imperceptible below voltages of 3V. The effect is reproduced in device CE4 at 77K in Figures 8a and b. Identical effects were observed at 4.2K. Conventional low power silicon bipolar transistors were measured to try to determine if the measurement equipment is responsible for the effect.

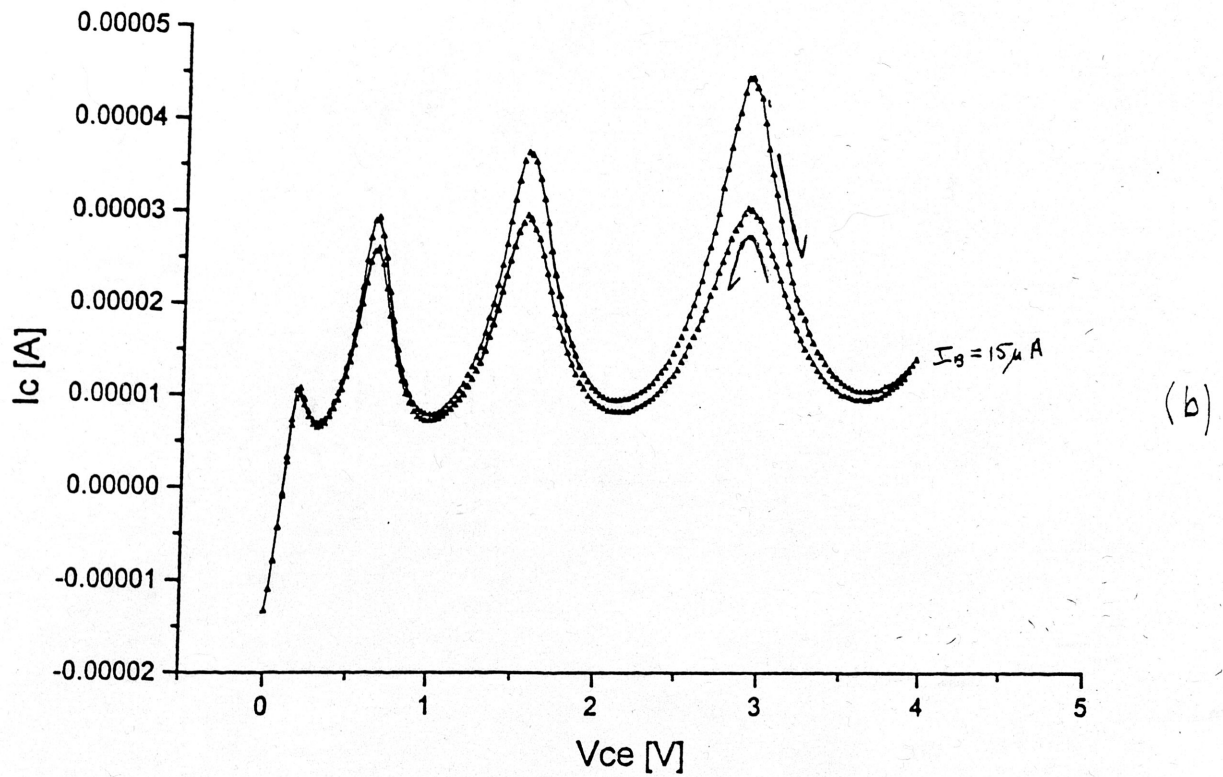
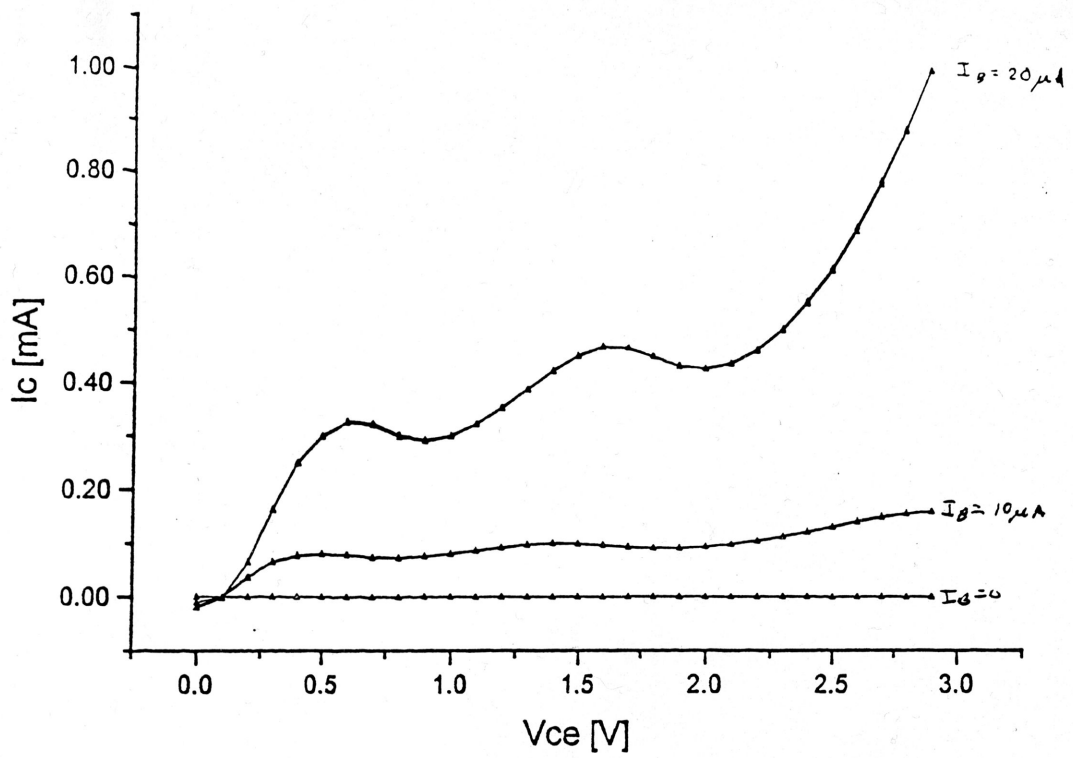


Figure 7. Common emitter I-V curves for device C4 at a) 300K, b) 77K.

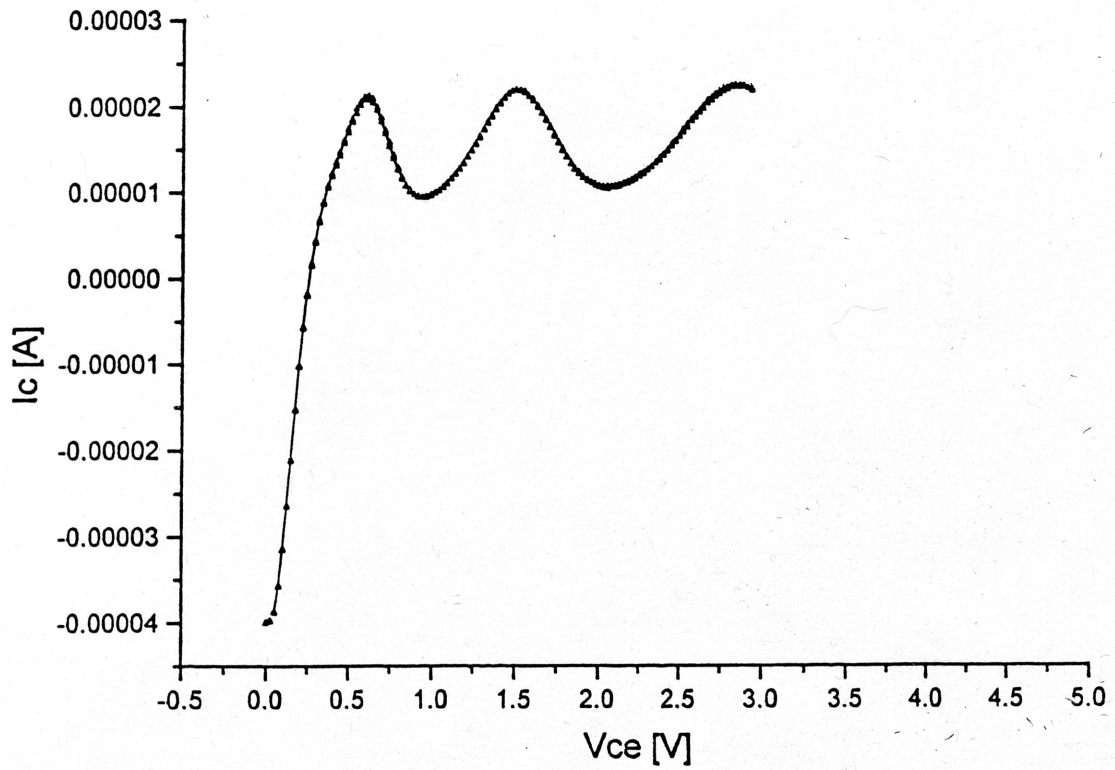
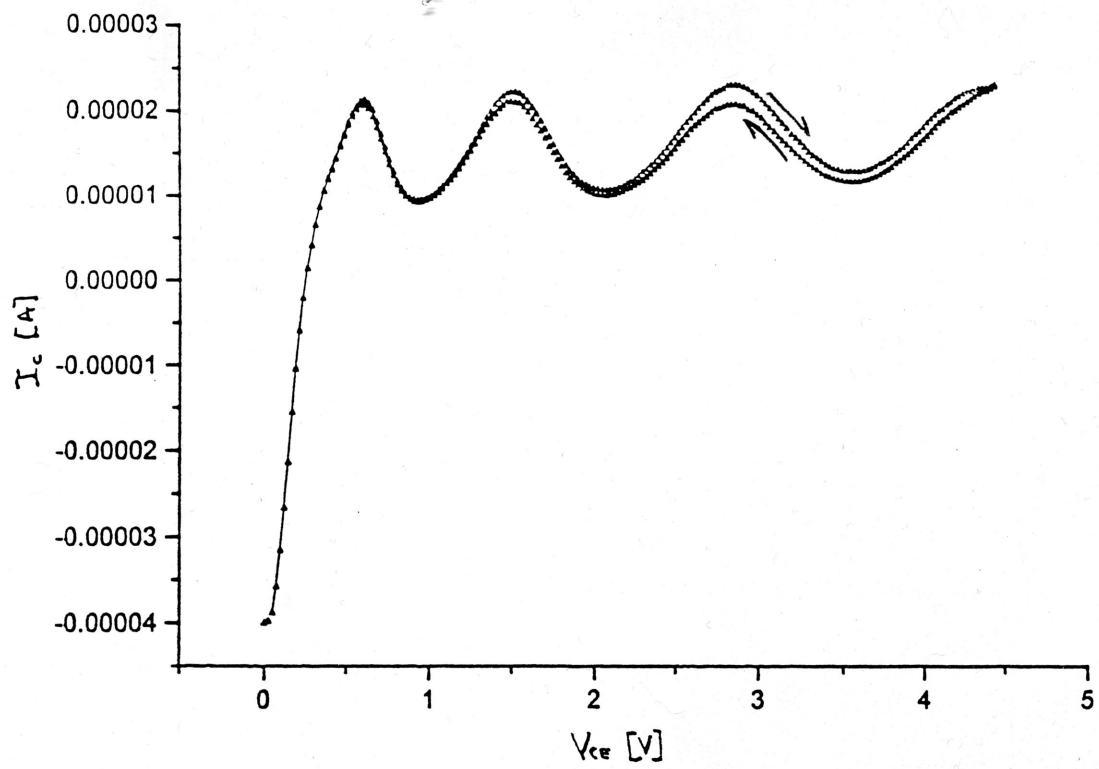


Figure 8. Common emitter I-V curves for device CE4 both at 77K.

No shifts were observed. Since these are DC measurements, and all measurement apparatus charge rates are on the order of milliseconds, combined with a slow data rate of one sample per three seconds suggests some other cause. Being such a strong function of the collector-emitter voltage, there might be a possibility of interplay between the reverse-biased collector heterojunction, and the hole accumulation layer on the inner interface of the collector tunnel barrier. At $V_{CE} > 3.5$ V, the electric field on the base side of the base-collector heterojunction may extend far enough into the base to decrease localization at this accumulation layer and thus produce a decrease in base resistance.

In Figures 9a and b, a different effect is observed: the shape of the individual peaks are a strong function of the applied base current, and appears to possess a weak temperature dependence, with the strongest effects at 80-90K. The cause of this anomalous behavior is not currently understood.

Upon completion of initial characterization, temperature studies were carried out on a single device, C4, since the others no longer functioned.

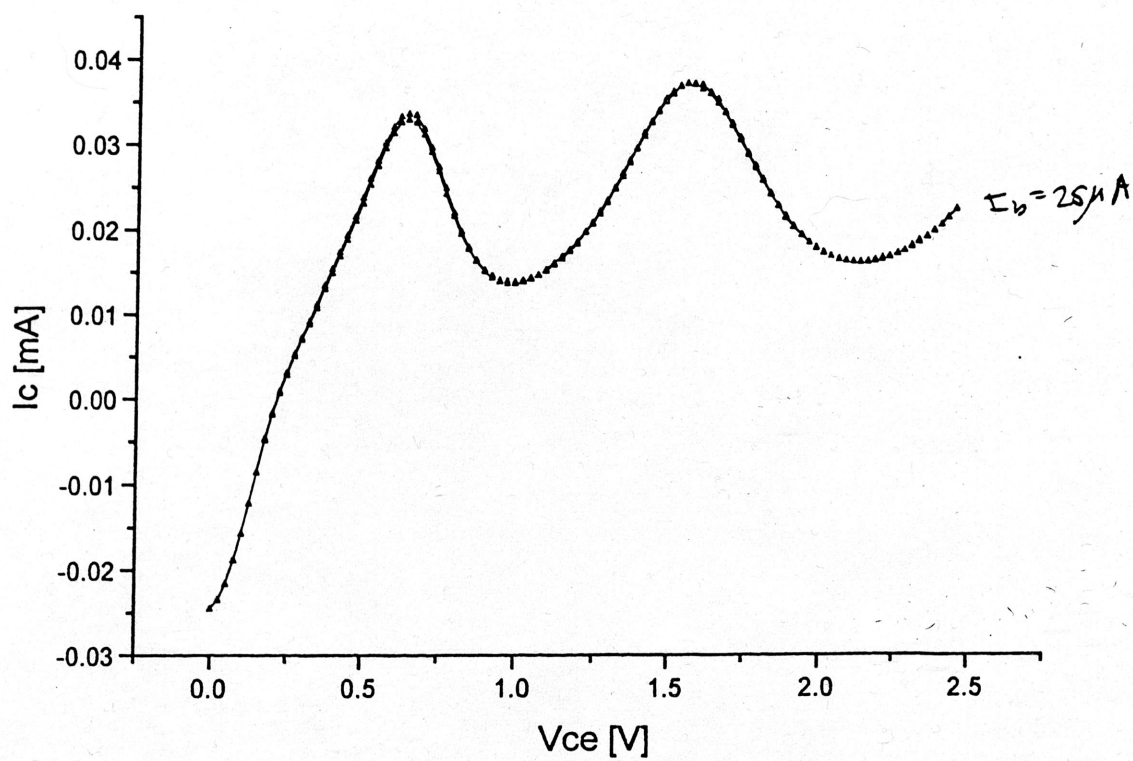
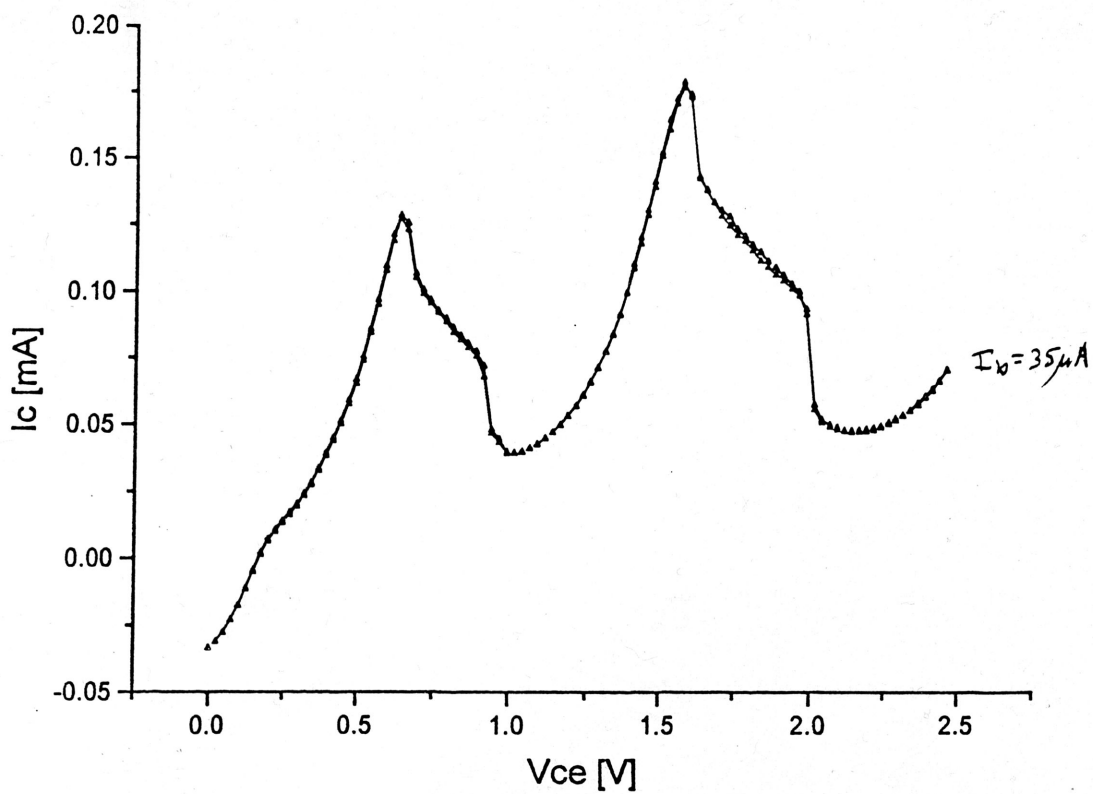


Figure 9. Common emitter I-V curves for device C8, at 77K.

Device C4 was measured over a range of temperatures from 4.2K to room temperature to study temperature dependence of the peak-to-valley ratio, peak amplitude, and any voltage shift in I-V curves. Collection of this data was difficult because the thermal mass of the probe made equilibrium times greater than twenty minutes, even for small changes in temperature and especially after a helium transfer. At most of the temperature points, repeated checking and resetting was required to obtain a given temperature. Additionally, the carbon-glass thermometer in the probe was not factory calibrated. A standard curve was supplied with 58 datapoints from 1.5K to 100K. The resistance vs T of this thermometer flattens out after 100K, complicating accurate measurements above that point.

Figure 10 shows the peak-to-valley ratio versus temperature from the second measurement run. The general trend of the data (decreasing P/V for increasing T) is not surprising, since lattice scattering due to phonons becomes more effective as the temperature is raised, and that the curve should begin to rise at the upper end of the temperature scale shown, due to thermal generation of carriers. But the deviations from this trend between 37K and 99K are as yet unexplained.

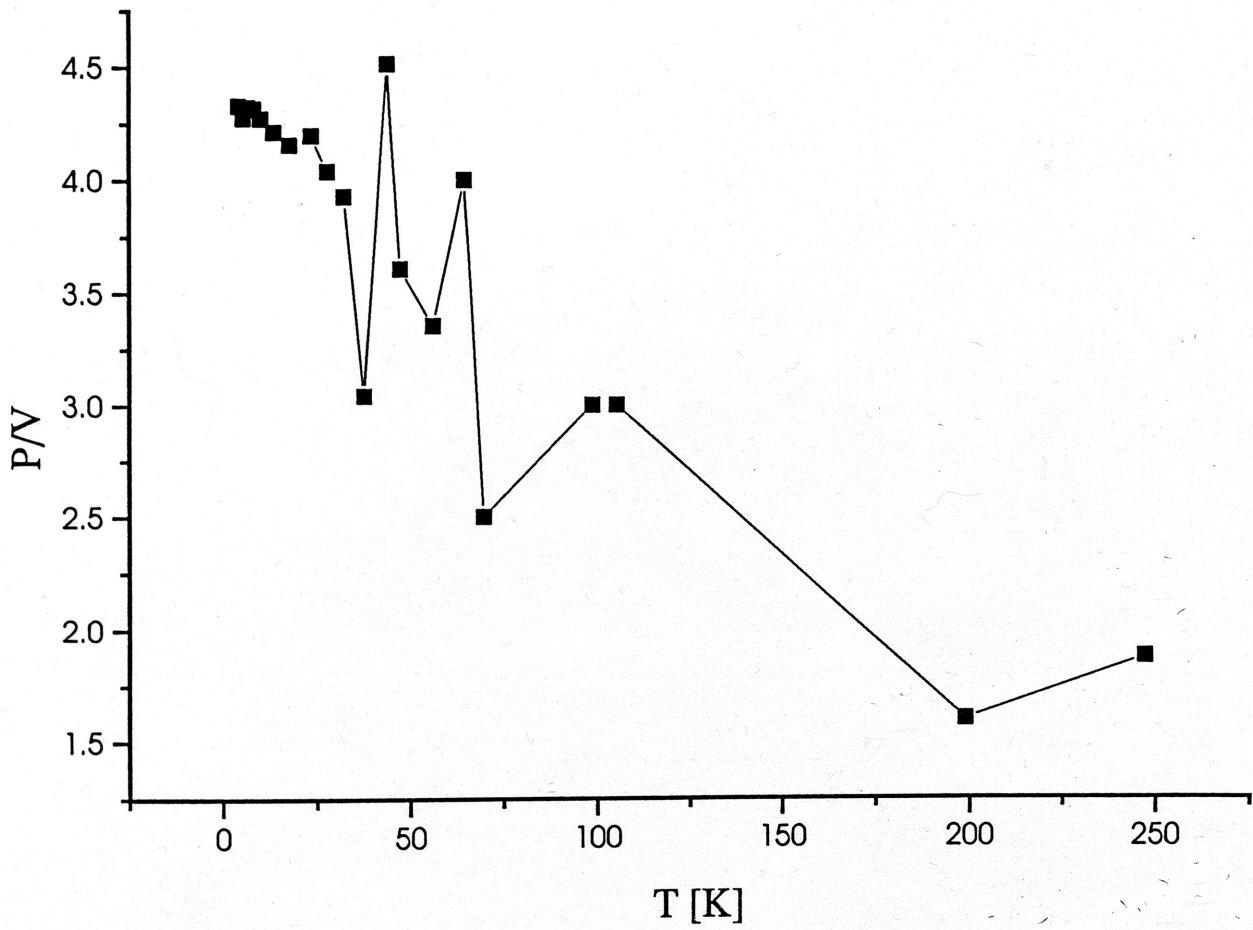


Figure 10. Peak-to-Valley ratio for device C4.

The peaks were found to be extremely stable with the collector-emitter voltage, with variations of less than 30mV. As in the first run, a maximum of four peaks were observed, but the collector-emitter voltage was kept to 2.5V or less for the remainder of the run, to avoid stressing the one remaining sample.

CHAPTER VII

CONCLUSIONS

Transport studies have been initiated on the BiQuaRTT. Observations have not, however, confirmed earlier reports on the number of peaks in the I-V curves.

Several previously unknown effects have been observed, but as of this writing, have yet to be explained. Further studies of these and newer sample devices are planned for Summer 1993 to attempt to resolve these issues.

REFERENCES

- [1] F. Capasso and R. A. Kiehl, *Appl. Phys.* 58, 1364 (1985).
- [2] M. Das in "HEMTs & HBTs: Devices, Fabrication, and Circuits", (F. Ali and A. Gupta, eds), Artech House, Boston, 1991.
- [3] S. Wang, "Semiconductor Device Physics Fundamentals," Prentice-Hall, New York, 1990.
- [4] F. Capasso, et. al., *IEEE Electron. Dev. Lett.* EDL-7, 573 (1986).
- [5] B. Ricc'o and M. Ya. Azbel, *Phys. Rev.* B29, 1970 (1984).
- [6] F. Capasso in "High Speed Semiconductor Devices," in (S.M. Sze, ed.), John Wiley and Sons, New York, 1990.
- [7] A. C. Seabaugh, et. al., *Appl. Phys. Lett.* 59, 26 (1991).
- [8] T. Tanoe, H. Mizuta, and S. Takahashi, *IEEE Electron. Dev. Lett.* EDL-9, 365 (1988).
- [9] A. Lakhani and R. Palmer, *Appl. Phys. Lett.*, 52, 1684 (1988).
- [10] R. Potter, et. al., *Appl. Phys. Lett.*, 52, 2163 (1988).
- [11] F. Capasso, et. al., *IEEE Electron. Dev. Lett.* EDL-8 297 (1987).
- [12] F. Capasso, et. al., *IEEE Trans. Electron Dev.* 36, 10 (1989).
- [13] W. Szott, Ph.D. dissertation, Texas A&M University, 1992 (unpublished).
- [14] D. Cahill, in "Experimental Techniques in Condensed Matter Physics at Low Temperatures," (R. Richardson and E. Smith, eds.), Addison-Wesley, Menlo Park, 1988.